

# Developing a Western Siberia reference site for tropospheric water vapour isotopologue observations obtained by different techniques (in-situ and remote sensing)

K. Gribanov<sup>1</sup>, J. Jouzel<sup>2</sup>, V. Bastrikov<sup>1,2,3</sup>, J.-L. Bonne<sup>2</sup>, F.-M. Breon<sup>2</sup>, M. Butzin<sup>4</sup>, O. Cattani<sup>2</sup>, V. Masson-Delmotte<sup>2</sup>, N. Rokotyan<sup>1</sup>, M. Werner<sup>4</sup>, and V. Zakharov<sup>1</sup>

<sup>1</sup>Climate and Environmental Physics Laboratory, Ural Federal University, Russia

<sup>2</sup>Institut Pierre Simon Laplace, Laboratoire des Sciences du Climat et de l'Environnement, France

<sup>3</sup>Institute of Industrial Ecology UB RAS, Russia

<sup>4</sup>Alfred Wegener Institute for Polar and Marine Research, Germany

**Abstract.** Water stable isotopologues provide integrated tracers of the atmospheric water cycle, affected by changes in air mass origin, non-convective and convective processes and continental recycling. Novel remote sensing and in situ measuring techniques have recently offered opportunities for monitoring atmospheric water vapour isotopic composition. Recently developed infrared laser spectrometers allow for continuous in situ measurements of surface water vapour  $\delta D_v$  and  $\delta^{18}O_v$ . So far, very few intercomparison of measurements conducted using different techniques have been achieved at a given location, due to difficulties intrinsic to the comparison of integrated with local measurements. Nudged simulations conducted with high resolution isotopically enabled GCMs provide a consistent framework for comparison with the different types of observations. Here, we compare simulations conducted with the ECHAM5-wiso model with two types of water vapour isotopic data obtained during summer 2012 at the forest site of Kourouka, Western Siberia: hourly ground-based FTIR total atmospheric columnar  $\delta D_v$  amounts, and in situ hourly Picarro  $\delta D_v$  measurements. There is an excellent correlation between observed and predicted  $\delta D_v$  at surface while the comparison between water column values derived from the model compares well with FTIR estimates.

## 1 Introduction

Owing to slight differences in the saturation vapour pressure and diffusivity in air of  $H_2^{16}O$ ,  $HD^{16}O$  and  $H_2^{18}O$  molecules, fractionation processes occur during phase changes of the water. As a result, the distribution of the water isotopologues (hereafter  $\delta D$  and  $\delta^{18}O$  expressed in ‰ versus VS-MOW (Craig, 1961)) varies both spatially and temporally in

the atmospheric water vapour and in the precipitation. Until recently, our knowledge of their present-day distribution has focused on precipitation, much easier to sample than atmospheric water vapour. This sampling difficulty partly explains why applications dealing with studies of atmospheric processes and atmospheric dynamics have long been limited while they have rapidly developed in such fields as isotope hydrology and isotope paleoclimatology (from ice cores and other archives).

The situation has recently changed thanks to technological advances which now allow for either in situ measurement or remote estimation of  $\delta D_v$  and  $\delta^{18}O_v$  in atmospheric water vapour. The quantification of water isotopologues in tropospheric water vapour based on space based remote sensing techniques pioneered by Zakharov et al. (2004) is now under rapid development (Worden et al., 2006; Payne et al., 2007; Nassar et al., 2007; Steinwagner et al., 2007; Frankenberg et al., 2009; Schneider and Hase, 2011; Frankenberg et al., 2012; Herbin et al., 2009; Field et al., 2012; Lacour et al., 2012; Boesh et al., 2013) and provides large scale, integrated measurements. Data from ground based high resolution Fourier Transform Infrared (FTIR) spectrometers have been exploited to retrieve information about vertical profiles of water stable isotopologues (mainly  $\delta D_v$ ) in water vapour from instruments both from the NDACC (Network for the Detection of Atmospheric Composition Change) sites (Schneider et al., 2006, 2010a,b, 2012) and columnar  $\delta D_v$  values from the TCCON (Total Carbon Column Observing Network) network (Boesh et al., 2013; Risi et al., 2012a).

A third major breakthrough has been accomplished when new infra red (IR) laser spectrometers have reached the same level of precision as mass spectrometers, and have become commercially available (Brand, 2009; Gupta et al., 2009). These devices are sufficiently robust to allow field measurements of the  $\delta D_v$  and  $\delta^{18}O_v$  composition of water vapour. After the development of calibration protocols, which require the introduction of reference waters and corrections for hu-

---

Correspondence to: K. Gribanov (kgribanov@remotesensing.ru)

midity and instrumental drift, such instruments have been deployed from tropical (Tremoy et al., 2012) to polar locations (Steen-Larsen et al., 2013) where they have revealed significant diurnal to seasonal variability in relationship with air mass origins, convection and surface-atmosphere moisture fluxes. Prior to the deployment of a network of stations where the  $\delta D_v$  and  $\delta^{18}O_v$  of surface water vapour will be continuously monitored, the information brought by water vapour stable isotopologues must be assessed for different climatic conditions.

In parallel, our ability to describe and simulate the distribution of water isotopologues using atmospheric general circulation models in which fractionation processes are embedded (IGCMs) has made considerable progress since the pioneering studies conducted in the eighties (Joussame et al., 1984; Jouzel et al., 1987). High resolution atmospheric models can now be nudged to atmospheric analyses products, allowing for precise comparisons with measurements in a consistent large scale meteorological framework. Sensitivity studies to uncertain atmospheric model parameterizations have shown the potential of water vapour isotopic data to constrain the representation of key processes linked to, e.g. cloud microphysics (Schmidt et al., 2005) or convection (Risi et al., 2012a).

In a comprehensive approach, Risi et al. (2012a,b) have brought together and compared satellite data sets from various instruments (SCIAMACHY, TES, ACE and MIPAS) and ground based remote sensing (FTIR at the NDACC and TCCON sites) and in situ techniques (surface vapour measurements and in situ aircraft data). From this comparison Risi et al. (2012a) extracted the most robust features and then used the LMDZ IGCM (LMDZiso) to understand and quantify the sources of differences between these data sets. They pointed out to significant differences between data sets but their common features appear to be remarkably well reproduced by LMDZiso in the lower and mid troposphere, at large scale. However, in Risi et al. (2012a), the amplitude of seasonal variations, the meridional isotopic gradient and the contrast between dry and convective tropical regions were underestimated by LMDZiso as well as by six other IGCMs involved in the SWING2 (Stable Water INtercomparison Group phase 2) intercomparison project.

Such data model intercomparison is a prerequisite if we want to use the variety of information on isotopic distribution in atmospheric water vapour (satellite data, ground based and in situ measurements) to diagnose biases in the representation of atmospheric processes in GCMs or infer information about, e.g. continental recycling. In their approach Risi et al. (2012b) aimed to use all available isotopic information with the consequence that the various data sets do not cover the same periods and the same locations, a difficulty which however is largely circumvented by applying a rigorous model-data comparison methodology.

Here, we propose a complementary approach which consists in focusing on one site, the Kourovka Observatory

(near Yekaterinburg, close to the western boundary of Western Siberia,  $57.038^\circ$  N,  $59.545^\circ$  S, see Fig. 1). This site is characterized by a well marked continental climate, with monthly mean temperatures varying from  $-16^\circ$  C (January) to  $+17^\circ$  C (July) and about 460 mm of annual precipitation, peaking in summer. It is affected by different air mass trajectories and summer continental precipitation recycling (Shalaumova et al., 2010). Its position in a pristine peatland and near the permafrost zone is strategic for the monitoring of the coupling between surface water and carbon budgets. At this site, we have access both to ground based (FTIR) and in situ vapour measurements (PICARRO L2130-i instrument). Comparison between different sets of  $\delta D$  were performed before, thus Lossow et al. (2011) compared between retrievals from different satellite sensors (Envisat/MIPAS, Odin/SMR, SCISAT/ACE-FTS), Schneider and Hase (2011) compared IASI and NDACC FTIR retrievals, Boesh et al. (2013) compared GOSAT short-wave infrared and TCCON FTIR retrievals, and Worden et al. (2006) compared TES retrievals with in-situ measurements. Here, we inter-compare two independent data sources (PICARRO and FTIR) using the outputs of the ECHAM5-wiso isotopic AGCM (T63) that has been run in a nudged version using ERA-Interim reanalysis fields (Dee et al., 2011; Berrisford et al., 2009). This inter-comparison will focus on a relatively short period between April and September 2012.

## 2 In situ isotopic measurements of surface water vapour

A Picarro laser instrument of type L2130-i was received by Ural Federal University in March 2012. Laboratory tests and further periodic calibration in the field were conducted in order to verify the reproducibility of the device using two different reference water samples: (i) DW (distilled water with  $\delta D = -96.4\text{‰}$ ); (ii) YEKA (mixing Antarctic snow with distilled water with  $\delta D = -289.0\text{‰}$ ). A third depleted reference sample (iii) DOMEQ (LSCE water standard with  $\delta D = -424.1\text{‰}$ ) was also used to assess the linearity of the system. Exact isotopic values of the reference water samples were measured at LSCE by IRMS.

The instrument was installed in Kourovka Observatory in mid March 2012, inside the same room as the FTIR spectrometer. Also the Kourovka site is equipped with Gill Instruments MetPak-II meteorological station which provides every second measurements of atmospheric pressure, wind speed and direction, air temperature and relative humidity. Air conditioning was set up to warrant stable temperatures inside the room (around  $18^\circ$  C). The sampling line consists of O'Brien optical quality stainless steel tubing (3/8 inch diameter) to minimize interactions between the sample and the tube. The length of the sampling line is 6 m, air being sampled about 8 ma.g.l. Self-regulating heating cable is used to keep stable temperature (around  $60^\circ$  C) along the sampling

line. The air input is protected against raindrops by a hard cover and against insects by a net. The station is implemented in the middle of a pine forest.

The measurement protocol consists of continuous ambient air measurements during 6 h, automatically switching to calibration with PICARRO Standard Delivery Module (SDM) performing a sequence of successive vaporization of DW and YEKA reference waters mixed with DRIERITE dried air during 30 min each. Altogether, each calibration sequence lasts about 60 min after accounting for pumping durations. Mean values and standard deviations in humidity and  $\delta D_v$  are calculated along the last 20 min of calibrations. Typically, standard deviations of 200 ppm and 1‰ respectively are reported for humidity levels around 15 000 ppm. As for the air measurements, after switching from calibration the instrument demonstrated very high variability in the measurement results because of residual traces of water from reference standards in the system. To account for this effect, air measurements were processed only after a time delay of 13 min. This time period was found appropriate for this particular PICARRO device during its installation and calibration.

These frequent calibrations allow to assess the stability of the measurements. Starting from June 2012, instabilities were identified during calibrations, due to leakage in one of the SDM syringes. This may lead to two biases: (i) fractionation in the syringe itself by exchange with ambient air, and (ii) introduction of air bubbles into the SDM and instabilities of injected flux and resulting measurements. The calibration module was subsequently replaced using a new type of glass syringe in September 2012, leading so far to very stable calibrations.

The quality of the post-processed data strongly depends on the stability of the calibrations. Water standard measurements are considered unstable and not taken into account when standard deviations of humidity and  $\delta D_v$  are above 600 ppm and 3‰, respectively. During the measurement period (from April to September) the total number of successful calibrations was 70 for DW and 130 for YEKA.

Fig. 2 shows the variability in the measured standards fitted with polynomial of 5th degree. Despite the presence of a certain gaps in calibrations due to the problems with power supply, leakage of SDM syringe and instability of SDM software, the overall drift of the system during 6 months is less than 5‰. Fitted polynomials were used for transferring the instrument isotopic values to the V-SMOW scale.

As it outlined by Steen-Larsen et al. (2013) isotopic measurements are sensitive to water vapour concentration, so it is required to establish calibration response functions as a function of humidity, based on measurement of reference waters injected at different humidity levels, from 1 000 to 25 000 ppm. These response functions were determined in-situ in April 2012. However for the period of interest we do not observe any significant effect on the measured  $\delta D_v$  values. Humidity level changes from 5 000 to 29 000 ppm with the mean

value of 14 000 ppm and this leads to variation in humidity-isotopologue response less than 3‰.

The overall calibration protocol used was realized according to the 6 step protocol, described in Steen-Larsen et al. (2013), except for the humidity correction that was not applied for this case.

Finally, we use both hourly and daily average values to present this data set and compare it with ECHAM5-wiso model results. For the period from 1 April to 30 September 2012 over which we will compare data and model results, 2476 hourly PICARRO measurements were produced which corresponds to 67 % of the total duration (3671 h). As FTIR (Sect. 4) data are specifically used to get information about  $\delta D_v$  in the water column, we will hereafter focus on this parameter both for the discussion of the dataset and its comparison with model results.

The currently available  $\delta D_v$  dataset extends to 21 November. We have, in Fig. 3, displayed both hourly individual measurements and a smooth curve (5 point running mean) limited to periods over which there are at least 6 hourly measurements successively. The amount of water vapour (as measured by the PICARRO instrument) has been reported on the same figure along with surface temperature using either measurements at the site available since 1 April or ERA-interim reanalysis data for the entire period (as used for the simulation).

As expected, the deuterium time series shows a clear seasonal cycle with its lowest values in spring (minimum  $-232‰$  on 5 April) and in fall (minimum  $-246‰$  on 18 November) and highest levels during summer ( $-103‰$  reached on 14 July and 11 August). While the highest monthly mean values are observed in June–August, the highest single hourly value is recorded to occur in spring ( $-92‰$  on 10 May). Indeed, large, and for some of them, rapid  $\delta D_v$  variations are superimposed on this seasonal cycle which will be fully described when winter data will be available. These fluctuations are more pronounced in fall with amplitudes reaching about 100‰ than during the summer during which no fluctuation exceeds 45‰. They are clearly related to large variations in temperature and to associated changes in the amount of water vapour,  $q_v$ .

Although much too simplistic, a Rayleigh type model helps to understand this link between  $\delta D_v$ , temperature and  $q_v$ . This model (Dansgaard, 1964) considers the isotopic fractionation occurring in an isolated air parcel in which the condensed phase is assumed to form in isotopic equilibrium with the surrounding vapour and to be removed immediately from the parcel. The isotopic composition of the water vapour at a given site,  $\delta D_v$ , is well approximated by:  $\delta D_v = ((1 + \delta D_0)(q_v/q_0)^{\alpha_m - 1}) - 1$ , in which  $\delta D_0$  and  $q_0$  are the deuterium content and the amount of water vapour at the oceanic origin of the air mass while  $\alpha_m$  stands for the average value of the fractionation coefficient between the oceanic source and the sampling site. Assuming no change in the conditions prevailing at the oceanic source (which again

is too simplistic) this should translate in a linear relationship between  $\ln(1 + \delta D_v)$  and  $\ln(q_v)$  while the link with site temperature results from the Clausius–Clapeyron equation.

With this in mind, we have plotted  $\ln(1 + \delta D_v)$  versus  $\ln(q_v)$  hourly (Fig. 4a) and daily (Fig. 4b) means and  $\delta D_v$  versus the site temperature using either hourly data for the period over which we have measurements at the site (Fig. 4c) or daily temperature in the Kourvka gridbox (Fig. 4d) as derived from reanalysis data (see Sect. 4.1). In line with the Rayleigh model in which the fraction of water remaining in the cloud is the primary driver of isotopic changes, there is a strong correlation ( $r^2 = 0.67$ ) between  $\ln(1 + \delta D_v)$  and  $\ln(q_v)$  for hourly data which increases ( $r^2 = 0.71$ ) when considering daily data and thus eliminating the diurnal cycle. The correlation of  $\delta D_v$  with temperature is weaker for hourly data either using local meteorological measurements ( $r^2 = 0.46$ ) or reanalysis data ( $r^2 = 0.49$ , not shown). It increases for daily data ( $r^2 = 0.72$ ) at a similar level as observed for  $\ln(q_v)$ .

### 3 Ground-Based FTIR

Ground-Based Fourier-Transform Infrared (FTIR) spectrometers are widely used for remote measurements of the atmospheric composition (Notholt and Scherms, 1994; Wunch et al., 2010, 2011; Hannigan et al., 2009). Data from the Ural Atmospheric Fourier Station (UAFS) in Kourvka astronomical observatory (57.048° N, 59.545° W, 270 m altitude, 80 km to the West from Yekaterinburg city) were used for comparison with ECHAM5-wiso output. UAFS provides high-resolution ground-based observations of atmospheric transmittance in the spectral region of 4000–11 000  $\text{cm}^{-1}$ . At TCCON sites, operating instruments are Bruker IFS-120HR and IFS-125HR (Wunch et al., 2010, 2011) which provide accurate and precise retrieval of column-averaged atmospheric concentrations of such gases as  $\text{CO}_2$ ,  $\text{CH}_4$ ,  $\text{H}_2\text{O}$ , HDO, etc. UAFS is equipped with Bruker IFS-125M mobile spectrometer (aligned by TCCON members in July 2012). At present, TCCON does not accept mobile versions of IFS-125 instruments but some studies show that they are able to achieve the required accuracy and precision ( $< 0.20\%$  for  $\text{XCO}_2$ , and  $< 0.16\%$  for  $\text{XCH}_4$ ) (Petri, 2012).

Columnar values of  $\delta D_v^{FTIR}$  were derived from total column abundances of HDO and  $\text{H}_2\text{O}$  retrieved from the spectra recorded from July 2012 to June 2013 in Kourvka. For data processing, the standard TCCON software GFIT was used (Wunch et al., 2010, 2011). GFIT retrieves the total number of molecules in the vertical atmospheric column, using the algorithm of profile scaling retrieval with the assumption that the shape of the profile of the retrieved gas is well known.  $\text{H}_2\text{O}$ , temperature and pressure a priori profiles are based on reanalysis data provided by National Centers for Environmental Prediction and the National Center for Atmospheric Research (NCEP/NCAR) (Kalnay et al., 1996). The

HDO a priori profile is calculated from  $\text{H}_2\text{O}$  profile as follows (Wunch et al., 2011):

$$x_{\text{HDO}}^{\text{apr}} = 0.16 x_{\text{H}_2\text{O}}^{\text{apr}} (8.0 + \log_{10}(x_{\text{H}_2\text{O}}^{\text{apr}})) \quad (1)$$

where  $x_{\text{HDO}}^{\text{apr}}$  is the a priori HDO volume mixing ratio (vmr) profile, and  $x_{\text{H}_2\text{O}}^{\text{apr}}$  is the a priori  $\text{H}_2\text{O}$  vmr profile. Examples for  $\text{H}_2\text{O}$  and corresponding  $\delta D_v^{FTIR}$  a priori profiles for each day of July 2012 are shown in Fig. 9. Microwindows containing saturated  $\text{H}_2\text{O}$  lines were excluded from final results to achieve more robust retrieval. As data base of spectral parameters, the revised water vapour line list was used (Shillings et al., 2011). To check the sensitivity of the retrieval to the a priori vertical profile of HDO, another retrieval run with constant  $\delta D_v$  a priori profile equal to zero (corresponding to natural abundance of HDO in the ocean) was performed. Fig. 5 shows a scatter plot for  $\delta D_v$  values retrieved using different a priori vertical profiles. This reveals that the retrieval of columnar  $\delta D_v$  values does not depend essentially on the initial guess.

## 4 The ECHAM isotopic model

### 4.1 Model setup

Atmospheric simulations were carried out using ECHAM5-wiso (Werner et al., 2011), which is the isotopologues-enhanced version of the atmospheric general circulation model ECHAM5 (Roeckner et al., 2003; Hagemann et al., 2006; Roeckner et al., 2006). Both stable water isotopologues  $\text{H}_2^{18}\text{O}$  and HDO have been explicitly implemented into its hydrological cycle (Werner et al., 2011) analogous to the isotope modelling approach used in the previous model releases ECHAM3 (Hoffmann et al., 1998) and ECHAM4 (e.g. Werner et al., 2001). For each phase of “normal” water (vapour, cloud liquid, cloud ice) being transported independently in ECHAM5, a corresponding isotopic counterpart is implemented in the model code. The isotopic and the “normal” water are described identically in the GCM as long as no phase transitions are concerned. Therefore, the transport scheme both for active tracers (moisture, cloud liquid water) and for the corresponding passive tracers (moisture, cloud water and cloud ice of the isotopologues) is the flux-form semi-Lagrangian transport scheme for positive definite variables implemented in ECHAM5 (Lin and Rood, 1996). Additional fractionation processes are defined for the water isotopologue variables whenever a phase change of the “normal” water occurs in ECHAM5. Two types of fractionation processes are considered in the model: equilibrium and non-equilibrium processes. An equilibrium fractionation takes place if the corresponding phase change is slow enough to allow full isotopic equilibrium. On the other hand non-equilibrium processes depend even on the velocity of the phase change, and therefore on the molecular diffusivity of

the water isotopologues. Processes which involve fractionation processes include the evaporation from the ocean, condensation either to liquid or to ice, as well as re-evaporation of liquid precipitation within the atmosphere. For evapotranspiration from land surfaces, possible isotopic fractionation is neglected (see Hoffmann et al. (1998) for detailed discussion of this issue).

ECHAM5-wiso has been validated with observations of isotopologue concentrations in precipitation and water vapour (Langebroeck et al., 2011; Werner et al., 2011). On a global and European scale, the annual as well as seasonal ECHAM-5-wiso simulation results are in good agreement with available observations from the Global Network of Isotopes in Precipitation, GNIP (IAEA-WMO, 2006). Furthermore, it has been shown that the simulation of water isotopologues in precipitation does clearly improve for an increased horizontal and vertical model resolution (Werner et al., 2011). The simulated near-surface isotopic composition of atmospheric water vapour  $\delta D_v$  is also in fairly good agreement with recent observations from five different GNIP stations. Model values and measurements agree well with differences in the range of  $\pm 10\%$ . A comparison of the ECHAM5-wiso simulations with total column averaged HDO data determined by the SCIAMACHY instrument on board the environmental satellite ENVISAT (Frankenberg et al., 2009) shows the same latitudinal gradients, but an offset between 20–50% of unknown origin. Focusing on Europe, the results by Langebroeck et al. (2011) indicate that variations of  $\delta^{18}O$  in precipitation are rather a regionally integrated signal of several climate variables than a proxy for either local temperature or precipitation changes. This finding is not just valid for ECHAM5-wiso results, but also supported by other modeling results (e.g. Schmidt et al., 2005) and confirmed by observational data (GNIP and ERA-40).

Based on our previous findings, we employ in this study the ECHAM5-wiso model with a medium-fine horizontal spectral resolution T63 (about  $1.9^\circ \times 1.9^\circ$ ). The vertical resolution is 31 hybrid levels. The model is forced with prescribed values of present-day insolation and greenhouse gas concentrations (IPCC, 2000), as well as with sea-surface temperatures and sea-ice concentrations according to ERA-Interim reanalysis data (Dee et al., 2011; Berrisford et al., 2009; data have been obtained from the ECMWF data server).

In order to allow a comparison with observations at the sub-seasonal scale, the ECHAM5-wiso model is nudged to reanalysis data, which ensures that the large scale atmospheric dynamics is correctly represented. Every six hours the dynamic-thermodynamic state of the model atmosphere is constrained to observations by implicit nudging (e.g. Krishnamurti et al., 1991; implemented by Rast, 2012), i.e. modeled fields of surface pressure, temperature, divergence and vorticity are relaxed to ERA-Interim reanalysis fields (Dee et al., 2011; Berrisford et al., 2009). If we compare climatological means of measured surface temperatures in Yekater-

inburg (Server, operated by the Space Monitoring Information Support laboratory, SMIS SRI RAS) with ERA-40 climatology data, we find a good agreement of the temperature seasonal cycle. The ERA-40 mean monthly surface temperatures show a small warm bias of less than  $1^\circ\text{C}$  for the period May–November, and slightly larger deviations ( $+1.0$  to  $+2.2^\circ\text{C}$ ) between December and April.

Although the hydrological cycle in our ECHAM5 setup is fully prognostic and not nudged to the ERA-Interim data, in Western Siberia the differences of the simulation results as compared to the hydrometeorological reanalysis fields are small. For instance, modelled daily precipitation agrees within  $1\text{mm day}^{-1}$  with reanalysis data, and the agreement with observations further improves if monthly averages are considered. The simulated total column water vapour (TCWV) tends to be systematically overestimated by 4–6 mm compared with reanalysis fields.

Our simulation starts on 1 January 2000, with an internal model time step of 12 min. For comparison with the available isotope observational records at Kourovka, we analyze simulation results for the period April to September 2012. We always evaluate model results with a temporal resolution of one hour, if not stated otherwise. For Kourovka, we are using values at the model grid point closest to the station.

For the period April to September 2012, an analysis of ERA-40 and ERA-interim surface temperature data reveals that the region around Kourovka station was anomalous warm, as compared to the long-time average temperatures (reference period 1960–1999). Strongest above-average warming with temperature anomalies of  $\approx +4^\circ\text{C}$  occurred in April and June, while in May and July temperatures were about  $1\text{--}2^\circ\text{C}$  warmer than average, only. For August, we find still an above-average warming of  $1\text{--}2^\circ\text{C}$  at Kourovka and adjacent regions of Western Siberia, but also cooler than average temperatures of the same order of magnitude in large parts of East Siberia. For September, temperatures in all Siberian regions have been anomalous warm by  $\approx 1\text{--}3^\circ\text{C}$  again.

## 4.2 Model results

We briefly describe the simulated near-surface temperature and surface pressure at the location of Kourovka (Fig. 6). A clear diurnal cycle is evidenced with typical day-versus-night temperature changes of  $\approx 5\text{--}10^\circ\text{C}$ . Superimposed on this diurnal cycle, the temperature record reveals strong variations within a timescale of a few days. These changes can be as large as  $10\text{--}15^\circ\text{C}$ . On the seasonal time scale, the difference between low temperature values in April and September, respectively, and the summer temperature maximum in mid-July to mid-August adds up to  $\approx 20^\circ\text{C}$ . This is slightly higher than the climatological observations from Yekaterinburg. Surface pressure at Kourovka varies between 960 hPa and 1000 hPa. This record also shows some multi-day variations but clearly lacks both a diurnal and seasonal cycle.

The simulated amount of water vapour  $q_v$  in the lowest atmospheric model layer also shows strong temporal variations at a time scale of a few days. While the water content in the air is rather low ( $3\text{--}6\text{ g kg}^{-1}$  air) between the beginning of April and early May, it rises thereafter to values of up to  $15\text{ g kg}^{-1}$  air. From mid-July to end of September, the simulated  $q_v$  values then fall back into the range  $5\text{--}10\text{ g kg}^{-1}$  air.

ECHAM5-wiso simulates surface-level water vapour  $\delta D_v$  values (hereafter  $\delta D_v$ ) mostly in the range  $-200$  to  $-100\text{‰}$  at the Kourovka site between April and September 2012 (Fig. 6). The model shows isotopic variations of  $30\text{--}50\text{‰}$  over a few days, over which are superimposed smaller short-term fluctuations lasting a few hours. The lowest  $\delta D_v$  values are found in early April and early May as well as in mid to late September, while summer  $\delta D_v$  values are less depleted. A distinct peak event in  $\delta D_v$  occurs between 30 August and 3 September.

Both the simulated  $\delta D_v$  values of the total water vapour column and  $\delta D$  in precipitation (not shown) are highly correlated with the simulated  $\delta D_v$  values near surface ( $r = 0.90$  and  $r = 0.97$ , respectively, for hourly values between 1 April and 30 September). Compared to the surface values, the  $\delta D_v$  signal of total water column is depleted by  $\approx 20\text{--}30\text{‰}$ . Precipitation occurs at 1216 1-h intervals between April and September (total number of 1-h intervals during this period: 4392) with a mean enrichment of  $\approx +70\text{‰}$  as compared to the surrounding vapour.

As seen in Fig. 6, the multi-day variations of  $\delta D_v$ ,  $q_v$  and surface pressure are strongly correlated. From our analyses, we find the strongest links between variations of temperature and water amount  $q_v$  ( $r = 0.70$ ), while variations of  $\delta D_v$  are only weakly linked to local temperature ( $r = 0.56$ ) and  $q_v$  ( $r = 0.60$ ). Our results support previous findings that  $\delta D_v$  variations on daily and synoptic time scales are often not strongly correlated with local temperature or water amount changes, but rather represent a more integrated signal of the climatic conditions during the transport of the vapour to a specific site (e.g. Schmidt et al., 2005; Langebroeck et al., 2011). Modeled surface pressure variations at Kourovka are neither strongly correlated to surface temperatures, water vapour, nor to  $\delta D_v$  (correlation coefficient  $|r| < 0.2$  in all cases).

In addition to  $\delta D$ , the isotopic signal of  $\delta^{18}\text{O}$  of the various water reservoirs and fluxes is also modeled within this ECHAM5-wiso simulation. At the grid point closest to Kourovka, we find a strong linear correlation between hourly values of  $\delta D_v$  and  $\delta^{18}\text{O}_v$  ( $r = 0.997$ ), with a slope of  $m = 7.99$  and a mean deuterium excess value  $d$  (defined as  $d = \delta D - 8 \times \delta^{18}\text{O}$ ) of  $+10.2\text{‰}$ . Between April and September, the modeled hourly excess values range between  $+5\text{‰}$  and  $+20\text{‰}$ . The potential use of the deuterium excess data to identify different transport regimes of moisture towards Kourovka will be investigated in detail in future studies.

From correlation analyses (not shown) of the simulated daily mean  $\delta D_v$  values at Kourovka and the isotopic composition at all other grid cells, we estimate that variations of isotope values in vapour at Kourovka are representative for isotopic changes in a region between  $45\text{--}75^\circ\text{ E}$  and  $48\text{--}66^\circ\text{ N}$ , with a correlation coefficient  $r$  higher than  $+0.5$ . A similar correlation pattern is found for variations of the water vapour amount  $q$ , but with slightly higher mean correlation coefficients ( $r \geq +0.65$ ). In contrast to these water quantities, the simulated near-surface temperature shows a much stronger and spatially extended correlation between Kourovka and its surroundings (mean  $r$  values  $> 0.9$ ).

## 5 Data comparison

### 5.1 Surface $\delta D_v$ : model data comparison

The ECHAM5-wiso results are first compared to the observed hourly water vapour PICARRO data  $q_v$  (Fig. 3c, red lines). The model correctly captures the patterns and magnitude of variability, with a very large correlation coefficient ( $r = 0.89$ ). Absolute values of water vapour measured with the PICARRO instrument are up to 20 % higher than the related model values. This might be explained by the facts, that the ECHAM5-wiso values represent the mean of the lowest atmospheric model level (surface to  $\approx 60\text{ m}$ ) while the PICARRO measurements were carried out at a height of 8 m, and that the closest model grid box has much larger size than point of in situ measurements and is located above complicated terrain containing small lakes and rivers with altitude differences about 400 m.

Simulated  $\delta D_v$  values are often  $30\text{--}40\text{‰}$  less depleted than the corresponding PICARRO data. This suggests a lack of depletion either along air mass trajectories or due to boundary layer mixing. Despite the systematic offset, a high correlation ( $r = 0.77$ ) is obtained between model and observed  $\delta D_v$  hourly variations. This result shows that the intra-seasonal  $\delta D_v$  variability at Kourovka is dominated by the synoptic variability, which is correctly resolved by the model in the nudged configuration.

The PICARRO data exhibit a stronger correlation between  $\delta D_v$  and  $q_v$  ( $r = 0.73$ ) than simulated ( $r = 0.60$ ). We note that this might be partly influenced by the lower number of measured data points ( $n = 3066$ ) as compared to the total number of hourly modeled values ( $n = 4392$ ) available for the period between April and September 2012. However, if we limit the analyses of the ECHAM5 values to those points in time, when PICARRO measurements exist, the simulated correlation between  $\delta D_v$  and  $q_v$  strengthens slightly ( $r = 0.61$ ), only.

The PICARRO observations and ECHAM5-wiso results consistently depict two pronounced  $\delta D_v$  negative excursions with minimum and maximum values of  $-200\text{‰}$  and  $-100\text{‰}$ , respectively, for the first days of April 2012 and

May 2012. Another negative excursion occurs on 12 September. Exemplarily, we have chosen the May event with highly depleted  $\delta D_v$  values between end of April and early May for a detailed analysis of the atmospheric conditions leading to this fast and strong isotope shift in vapour at Kourovka (Fig. 7). In the model framework, the minimum in  $\delta D_v$  lags a local surface pressure minimum by 1 day and precedes a drop in surface air temperature, which reaches its lowest temperatures 4 days later. This sequence of events suggests that such  $\delta D_v$  variations at Kourovka are related to passages of dynamic low and high pressure systems and advection of remote air masses. This hypothesis is further investigated by analysis of the isobaric flow at 850 hPa. A few days before this depletion event, the Kourovka area was receiving southwesterly air masses transporting relatively warm and enriched vapour (Fig. 8, top panel). Around 1 May, the atmospheric circulation changed due to a pronounced low pressure system north of Kourovka. As a result, the main air flow was then transported from central Siberia with depleted  $\delta D_v$  levels (Fig. 8, middle panel). During the following days, this northerly airflow caused the cooling at Kourovka. Starting from 7 May, a new high pressure system south of Kourovka was again dominating the atmospheric flow pattern, bringing warm and relatively enriched vapour to this region (Fig. 8, bottom panel). These simulated changes in atmospheric transport to Kourovka between 20 April and 11 May are in good agreement with back trajectory analyses of air masses, available from the AERONET (2012) for the location of Yekaterinburg (not shown).

We conclude that PICARRO measurements and ECHAM5-wiso simulation results of  $\delta D_v$  and related quantities (vapour  $q$ , surface temperature) between April and September 2012 are in good agreement. Even short-term isotope variations occurring on an hourly time scale are correctly reproduced in this nudged simulation. Thus, one may safely use the ECHAM5-wiso model results for an improved interpretation of observed isotopic variations near Kourovka in future studies.

## 5.2 Comparison of FTIR data with measured at surface and model data

Since the model provides hourly-averaged output data, data retrieved from FTIR measurements taken within 1 h were also averaged. For the comparison between model and FTIR observations we assume that the modeled HDO and H<sub>2</sub>O profiles are true, and we smooth original model values by applying the following equation (Rodgers and Connor, 2003; Risi et al., 2012a):

$$Q = \sum_{i=1}^n \frac{\Delta P_i}{g} (A_i * q_i^{\text{sim}} + (1 - A_i) q_i^{\text{apr}}) \quad (2)$$

Here,  $Q$  is the retrieved total column mass of HDO or H<sub>2</sub>O, respectively,  $q^{\text{sim}}$  is the specific humidity profile simulated by the model for atmospheric layer  $i$ ,  $q^{\text{apr}}$  is the specific

humidity in the same layer according to the a priori profile used in the retrieval (converted from wet to dry-mole fractional values according to Wunch et al., 2010),  $A_i$  is the  $i$ -th component of the column averaging kernel vector,  $\Delta P_i$  is the thickness of the  $i$ -th atmospheric layer,  $g$  is the gravity acceleration. Column averaging kernel as a function of pressure for different solar zenith angles of measurements are shown in Fig. 10. TCCON a priori and averaging kernel profiles are tabulated using a different vertical coordinate system than the model profiles (71 pressure levels versus 31 hybrid layers). To ensure numerical consistency, model profiles were interpolated to the same vertical resolution as averaging kernel (71 pressure levels) before the vertical integration was carried out. The  $\delta D_v^{\text{FTIR}}$  of total column water vapour ( $\delta D_{\text{TCVW}}$ ) was then calculated from the normalized ratio of  $Q_{\text{HDO}}$  and  $Q_{\text{H}_2\text{O}}$ .

To check how retrieved columnar  $\delta D_v^{\text{FTIR}}$  values correlate to collocated ground  $\delta D_v$  values we selected FTIR and extended until April 2013 PICARRO measurements taken within the same hours.

Before we enter the comparison between smoothed ECHAM5-wiso results and observations, we consider the effect of the applying column averaging kernels to the original model results. In Kourovka, it shifts the original model results for  $\delta D_{\text{TCVW}}$  to more positive values by about 9‰ in the average, and also induces a change of the expected slope between smoothed and originally simulated  $\delta D_{\text{TCVW}}$  from 1.0 to 0.87. The positive shift of retrieval values is essentially a consequence of the fact that between 1000 and 200 hPa, the isotopic ratio of TCCON a priori profiles is systematically higher than in the ECHAM simulations. The change of the slopes deserves further investigation.

FTIR measurements were carried out in Kourovka on 32 days during one year since July 10, 2012 until June 30, 2013. Retrieved values of  $\delta D_v^{\text{FTIR}}$  range from  $-316$ ‰ on February 22, 2013 to  $-40$ ‰ on June 12, 2013. Multiple measurements on July 10, 2012 record an increase of  $\delta D_v^{\text{FTIR}}$  from morning to noon by about 15‰. Observations and retrieved model results are correlated with  $r^2 = 0.84$  and scatter with an absolute standard deviation of 22‰ (see Fig. 11a). We do not find any systematic trend underlying the differences. The observations are systematically shifted to the higher values comparing to the model results and have larger amplitude of variations (by approximately 30 percent). It can be explained by the uncertainties and incorrect temperature dependence in spectroscopic line parameters in the linelist. The measured increase of  $\delta D_v^{\text{FTIR}}$  during 10 July, 2012 is also found in the model results but with a smaller amplitude (10‰). In the model, this fast isotopic enrichment coincides with the temporal evolution of lower tropospheric temperatures, exhibiting for Kourovka a pronounced diurnal cycle during the summer months. Given the limited number of observations that are available so far, a rigid interpretation and assessment FTIR measurements from Kourovka has to be postponed to the future with more detailed investigation of retrieval sensi-

tivity and cross-dependance on humidity.

The comparison of hourly averaged columnar FTIR measurements with hourly averaged PICARRO ground measurements shows correlation  $r^2 = 0.84$  (see Fig. 11b). Amplitude of seasonal variations of the retrieved  $\delta D_v^{FTIR}$  is approximately 2 times larger than that of  $\delta D_v$  values measured by PICARRO at surface.

## 6 Conclusions

The present study is part of a project aiming to investigate the water and carbon cycles in permafrost regions and pristine peatlands of Western Siberia and their projected changes under a warming climate. The isotopic approach is a key element of this project and the results that we have presented and discussed in this article should be considered as a first and necessary step to fully exploit the isotopic information contained in water vapour. To this end we have combined two independent methods to acquire data (continuous surface measurements and FTIR) and evaluate them against the results derived from a dedicated simulation of the ECHAM5-wiso IGCM focusing on this region.

As expected from a Rayleigh type model, and generally observed in middle and high latitude regions (Rozanski et al., 1992), a significant part of the daily isotopic variations ( $\delta D_v$ ) observed in Kourouka water vapour is explained by local changes in the amount of water vapour ( $r^2 = 0.71$ ) and temperature ( $r^2 = 0.72$ ). Obviously, a general circulation model which accounts for the origin of the water vapour, for the complexity of weather situations and for the differences of associated fractionations (e.g convective versus non-convective systems) is a more appropriate tool to examine the link between  $\delta D_v$  and climatic parameters. There is indeed an excellent correlation between observed and predicted  $\delta D_v$  values including for rapid excursions related to concurrent changes in atmospheric circulation.

This data model comparison fully justifies the use of ECHAM5-wiso to evaluate the method based on the exploitation of FTIR data, allowing remote measurements of  $\delta D_v$  in the water column. The method is very satisfying although being limited to a small number of days.

To sum up, the  $\delta D_v$  comparison between two observational approaches and a medium-high resolution IGCM, undertaken for the first time at a given site, is quite promising. Data acquisition with the Picarro instrument will be now performed on a continuous basis and a second instrument will be deployed in summer 2013 at Labytnangi located near the Arctic circle ( $66^\circ 39' N$ ,  $66^\circ 23' E$ , see Fig. 1) with the aim to contribute to an Arctic network now under development. Further work will include the exploitation of oxygen-18 and associated deuterium excess from the PICARRO data, a comparison of the algorithm developed to infer column  $\delta D_v$  from the GOSAT thermal infrared band and the method currently applied in the short-wave infrared (Frankenberg et al., 2012),

as well as the development of an improved algorithm to exploit FTIR data for isotopic purposes. At last the use of a second IGCM (LMDZiso) should help to interpret these data in a larger geographical context.

*Acknowledgements.* This research was supported by the grant of Russian government under the contract 11.G34.31.0064 and RFBR grant No. 12-01-00801-a. We acknowledge to Hans Christian Steen-Larsen for fruitful discussions on measurements techniques and calibrations. Zakharov, V. I. and Rokotyanyan, N. V. thank Igor Ptashnik for fruitful discussions regarding impact of error of spectral parameters of target molecules on precision of the retrieval and his suggestion to use the revised water line list.

## References

- Aerosol Robotic Network (AERONET): [http://aeronet.gsfc.nasa.gov/new\\_web/index.html](http://aeronet.gsfc.nasa.gov/new_web/index.html), last access: 1 July 2012.
- Berrisford, P., Dee, D., Fielding, K., Fuentes, M., Kallberg, P., Kobayashi, S., and Uppala, S.: The ERA-Interim archive, ERA Report Series, European Centre for Medium Range Weather Forecast, Shinfield Park, Reading, Berkshire RG29AX, United Kingdom, August 2009.
- Boesh, H., Deutscher, N. M., Warneke, T., Byckling, K., Coogan, A. J., Griffith, D. W. T., Notholt, J., Parker, R. J., and Wang, Z.: HDO/H<sub>2</sub>O ratio retrievals from GOSAT, Atmos. Meas. Tech., 6, available at: <http://www.atmos-meas-tech.net/6/599/2013/>, 2013.
- Brand, W. A.: Maintaining high precision of isotope ratio analysis over extended periods of time, Isot. Environ. Health S., 45, 135–149, available at: <http://www.ncbi.nlm.nih.gov/pubmed/20183227>, 2009.
- Collard, A.D.: Selection of IASI channels for use in numerical weather prediction, Q.J.R.Meteorol.Soc., 133, 1977–1991, 2007.
- Craig, H.: Standard for reporting concentrations of deuterium and oxygen-18 in natural waters, Science, 133, 1833–1834, available at: <http://www.ncbi.nlm.nih.gov/pubmed/17819002>, 1961.
- Dansgaard, W.: Stable isotopes in precipitation, Tellus, 16, 436–468, available at: <http://doi.wiley.com/10.1111/j.2153-3490.1964.tb00181.x>, 1964.
- Dee, D. P., Uppala, S. M., Simmons, A. J., Berrisford, P., Poli, P., Kobayashi, S., Andrae, U., Balmaseda, M. A., Balsamo, G., Bauer, P., Bechtold, P., Beljaars, A. C. M., van de Berg, L., Bidlot, J., Bormann, N., Delsol, C., Dragani, R., Fuentes, M., Geer, A. J., Haimberger, L., Healy, S. B., Hersbach, H., Hólm, E. V., Isaksen, I., Kållberg, P., Köhler, M., Matricardi, M., McNally, A. P., Monge-Sanz, B. M., Morcrette, J.-J., Park, B.-K., Peubey, C., de Rosnay, P., Tavolato, C., Thépaut, J.-N., and Vitart, F.: The ERA-Interim reanalysis: configuration and performance of the data assimilation system, Q. J. Roy. Meteor. Soc., 137, 553–597, 2011.
- ECMWF data server: <http://data-portal.ecmwf.int/>, last access: 30 September 2012.
- Frankenberg, C., Yoshimura, K., Warneke, T., Aben, I., Butz, A., Deutscher, N., Griffith, D., Hase, F., Notholt, J., Schneider, M., Schrijver, H., and Röckmann, T.: Dynamic processes governing lower-tropospheric HDO/H<sub>2</sub>O ratios as observed from space



- and ground, *Science*, 325, 1374–1377, available at: <http://www.sciencemag.org/content/325/5946/1374.short>, 2009.
- Frankenberg, C., Wunch, D., Toon, G., Risi, C., Scheepmaker, R., Lee, J.-E., Wennberg, P., and Worden, J.: Water vapor isotopologues retrievals from high resolution GOSAT short-wave infrared spectra, *Atmos. Meas. Tech. Discuss.*, 5, 6357–6386, doi:<http://dx.doi.org/10.5194/amtd-5-6357-2012>, 2012.
- Field, R. D., Risi, C., Schmidt, G. A., Worden, J., Voulgarakis, A., LeGrande, A. N., Sobel, A. H., and Healy, R. J.: A Tropospheric Emission Spectrometer HDO/H<sub>2</sub>O retrieval simulator for climate models, *Atmos. Chem. Phys.*, 12, 10485–10504, doi:<http://dx.doi.org/10.5194/acp-12-10485-2012>, 2012.
- Gupta, P., Noone, D., Galewsky, J., Sweeney, C., and Vaughn, B. H.: Demonstration of high-precision continuous measurements of water vapor isotopologues in laboratory and remote field deployments using wavelength-scanned cavity ring-down spectroscopy (WS-CRDS) technology, *Rapid Commun. Mass Sp.*, 23, 2534–2542, available at <http://www.ncbi.nlm.nih.gov/pubmed/19603459>, 2009.
- Hagemann, S., Arpe, K., and Roeckner, E.: Evaluation of the hydrological cycle in the ECHAM5 model, *J. Climate*, 19, 3810–3827, 2006.
- Hannigan, J. W., Coffey, M. T., and Goldman, A.: Semi-autonomous FTS ObservaLon system for remote sensing of stratospheric and tropospheric gases, *J. Atmos. Ocean Tech.*, 26, 1814–1828, doi:10.1175/2009JTECHA1230.1, 2009.
- Herbin, H., Hurtmans, D., Clerbaux, C., Clarisse, L., and Coheur, P.-F.: H<sub>2</sub><sup>16</sup>O and HDO measurements with IASI/MetOp, *Atmos. Chem. Phys.*, 9, 9433–9447, doi:<http://dx.doi.org/10.5194/acp-9-9433-2009>, 2009.
- Hoffmann, G., Werner, M., and Heimann, M.: Water isotope module of the ECHAM atmospheric general circulation model: a study on timescales from days to several years, *J. Geophys. Res.*, 103, 16871–16896, available at: <http://www.agu.org/pubs/crossref/1998/98JD00423.shtml>, 1998.
- IAEA-WMO, Global Network of Isotopes in Precipitation: The GNIP Database: [http://www-naweb.iaea.org/naweb/ihs/resources\\_gnip.html](http://www-naweb.iaea.org/naweb/ihs/resources_gnip.html), last access: 20 December 2012, 2006.
- Joussame, S., Sadourny, R., Jouzel, J.: A general circulation model of water isotope cycles in the atmosphere, *Nature*, 311, 24–29, 1984.
- Jouzel, J., Russell, G. L., Suozzo, R. J., Koster, R. D., White, J. W. C., and Broecker, W. S.: Simulations of the HDO and H<sub>2</sub><sup>18</sup>O atmospheric cycles using the NASA GISS General Circulation Model: the seasonal cycle for present-day conditions, *J. Geophys. Res.*, 92, 14739–14760, 1987.
- Kalnay, E., Kanamitsu, M., Kistler, R., Collins, W., Deaven, D., Gandin, L., Iredell, M., Saha, S., White, G., Woollen, J., Zhu, Y., Leetmaa, A., and Reynolds, R.: The NCEP/NCAR 40-year reanalysis project, *B. Am. Meteorol. Soc.*, 77, 437–471, 1996.
- Krishnamurti, T. N., Xue, J., Bedi, H. S., Ingles, K., and Oosterhof, D.: Physical initialization for numerical weather prediction over the tropics, *Tellus*, 43AB, 53–81, 1991.
- Lacour, J.-L., Risi, C., Clarisse, L., Bony, S., Hurtmans, D., Clerbaux, C., and Coheur, P.-F.: Mid-tropospheric  $\delta$ D observations from IASI/MetOp at high spatial and temporal resolution, *Atmos. Chem. Phys.*, 12, 10817–10832, doi:10.5194/acp-12-10817-2012, 2012.
- Langebroeck, P. M., Werner, M., and Lohmann, G.: Climate information imprinted in oxygen-isotopic composition of precipitation in Europe, *Earth Planet. Sc. Lett.*, 311, 144–154, 2011.
- Nakicenovic, N. and Swart, R. (Eds.): IPCC Special Report on Emissions Scenarios, IPCC, Cambridge University Press, Cambridge, UK, 2000.
- Lin, S.-J. and Rood, R. B.: Multidimensional flux-form semi-Lagrangian transport schemes, *Mon. Weather Rev.*, 124, 2046–2070, 1996.
- Lossow, S., Steinwagner, J., Urban, J., Dupuy, E., Boone, C. D., Kellmann, S., Linden, A., Kiefer, M., Grabowski, U., Glatztor, N., Hpfner, M., Rckmann, T., Murtagh, D. P., Walker, K. A., Bernath, P. F., von Clarmann, T., and Stiller, G. P.: Comparison of HDO measurements from Envisat/MIPAS with observations by Odin/SMR and SCISAT/ACE-FTS, *Atmos. Meas. Tech.*, 4, 1855–1874, available at <http://www.atmos-meas-tech.net/4/1855/2011/>, 2011.
- Nassar, R., Bernath, P. F., Boone, C. D., Gettelman, A., McLeod, S. D., and Rinsland, C. P.: Variability in HDO/H<sub>2</sub>O abundance ratios in the tropical tropopause layer, *Journal of Geophysical Research*, 112, 1–11, doi:10.1029/2007JD008417, 2007.
- Notholt, J. and Schrems, O.: Ground-based FTIR measurements of vertical column densities of several trace gases above Spitsbergen, *Geophysical Research Letters*, 21, 1355–1358, 1994.
- Payne, V. H., Noone, D., Dudhia, A., Piccolo, C., and Grainger, R. G.: Global satellite measurements of HDO and implications for understanding the transport of water vapour into the, *Q. J. Roy. Meteor. Soc.*, 133, 1459–1471, doi:10.1002/qj.127, 2007.
- Petri, C.: Ground-based remote sensing of CO<sub>2</sub> and CH<sub>4</sub> using a Bruker 120/5 M FTS, IRWG/TCCON meeting, Wengen, Switzerland, 11–15 June 2012.
- Rast, S.: Sea ice and nudging in ECHAM5, available at: <http://www.mpimet.mpg.de/en/staff/sebastian-rast/echam-special-documentation.html>, last access: 8 December 2012.
- Risi, C., Noone, D., Worden, J., Frankenberg, C., Stiller, G., Kiefer, M., Funke, B., Walker, K., Bernath, P., Schneider, M., Wunch, D., Sherlock, V., Deutscher, N., Griffith, D., Wennberg, P. O., Strong, K., Smale, D., Mahieu, E., Barthlott, S., Hase, F., García, O., Notholt, J., Warneke, T., Toon, G., Sayres, D., Bony, S., Lee, J., Brown, D., Uemura, R., and Sturm, C.: Process-evaluation of tropospheric humidity simulated by general circulation models using water vapor isotopologues: 1. Comparison between models and observations, *J. Geophys. Res.*, 117, D05303, doi:10.1029/2011JD016621, 2012a.
- Risi, C., Noone, D., Worden, J., Frankenberg, C., Stiller, G., Kiefer, M., Funke, B., Walker, K., Bernath, P., Schneider, M., Bony, S., Lee, J., Brown, D., and Sturm, C.: Process-evaluation of tropospheric humidity simulated by general circulation models using water vapor isotopic observations: 2. Using isotopic diagnostics to understand the mid and upper tropospheric moist bias in the tropics and subtropics, *J. Geophys. Res.*, 117, D05304, doi:10.1029/2011JD016623, 2012b.
- Rodgers, C. D. and Connor, B. J.: Intercomparison of remote sounding instruments, *J. Geophys. Res.*, 108, 4116, doi:10.1029/2002JD002299, 2003.

- Roeckner, E., Bäuml, G., Bonaventura, L., Brokopf, R., Esch, M., Giorgetta, M., Hagemann, S., Kirchner, I., Kornblüeh, L., Manzini, E., Rhodin, A., Schlese, U., Schulzweida, U., and Tompkins, A.: The atmospheric general circulation model ECHAM5, Part 1, Model description, Report No. 349, Max Planck Institute for Meteorology, Hamburg, Germany, 2003.
- Roeckner, E., Brokopf, R., Esch, M., Giorgetta, M., Hagemann, S., Manzini, E., Schlese, U., and Schulzweida, U.: Sensitivity of simulated climate to horizontal and vertical resolution in the ECHAM5 atmosphere model, *J. Climate*, 19, 3771–3791, 2006.
- Rozanski, K., Araguás-Araguás, L., and Gonfiantini, R.: Relation between long-term trends of oxygen-18 isotope composition of precipitation and climate, *Science*, 258, 981–985, available at: <http://www.ncbi.nlm.nih.gov/pubmed/17794595>, 1992.
- Russia's Weather Server – Weather Archive: <http://meteo.infospace.ru/wcarch/html/index.sht>, last access: 1 December 2012.
- Schmidt, G. A., Hoffmann, G., Shindell, D. T., and Hu, Y.: Modeling atmospheric stable water isotopes and the potential for constraining cloud processes and stratosphere-troposphere water exchange, *J. Geophys. Res.*, 110, D21314, doi:10.1029/2005JD005790, 2005.
- Schneider, M., and Hase, F.: Optimal estimation of tropospheric H<sub>2</sub>O and δD with IASI/METOP, *Atmos. Chem. Phys.*, 11, 11207–11220, available at: <http://www.atmos-chem-phys.net/11/11207/2011/>, 2011.
- Schneider, M., Hase, F., and Blumenstock, T.: Ground-based remote sensing of HDO/H<sub>2</sub>O ratio profiles: introduction and validation of an innovative retrieval approach, *Atmos. Chem. Phys.*, 6, 4705–4722, doi:10.5194/acp-6-4705-2006, 2006.
- Schneider, M., Toon, G. C., Blavier, J.-F., Hase, F., and Leblanc, T.: H<sub>2</sub>O and δD profiles remotely-sensed from ground in different spectral infrared regions, *Atmos. Meas. Tech.*, 3, 1599–1613, doi:10.5194/amt-3-1599-2010, 2010a.
- Schneider, M., Sepúlveda, E., García, O., Hase, F., and Blumenstock, T.: Remote sensing of water vapour profiles in the framework of the Total Carbon Column Observing Network (TCCON), *Atmos. Meas. Tech.*, 3, 1785–1795, doi:10.5194/amt-3-1785-2010, 2010b.
- Schneider, M., Barthlott, S., Hase, F., González, Y., Yoshimura, K., García, O. E., Sepúlveda, E., Gomez-Pelaez, A., Gisi, M., Kohlhepp, R., Dohe, S., Blumenstock, T., Wiegeler, A., Christner, E., Strong, K., Weaver, D., Palm, M., Deutscher, N. M., Warneke, T., Notholt, J., Lejeune, B., Demoulin, P., Jones, N., Griffith, D. W. T., Smale, D., and Robinson, J.: Ground-based remote sensing of tropospheric water vapour isotopologues within the project MUSICA, *Atmos. Meas. Tech.*, 5, 3007–3027, doi:10.5194/amt-5-3007-2012, 2012.
- Shalaumova, Yu. V., Fomin, V. V., and Kapralov, D. S.: Spatiotemporal dynamics of the Urals climate in the second half of the 20th century, *Russ. Meteorol. Hydrol.*, 35, 107–114, 2010.
- Shillings, A. J. L., Ball, S. M., Barber, M. J., Tennyson, J., and Jones, R. L.: An upper limit for water dimer absorption in the 750 nm spectral region and a revised water line list, *Atmos. Chem. Phys.*, 11, 4273–4287, doi:10.5194/acp-11-4273-2011, 2011.
- Steen-Larsen, H. C., Masson-Delmotte, V., Sjolte, J., Johnsen, S. J., Vinther, M. B., Bréon, F.-M., Clausen, H. B., Dahl-Jensen, D., Falourd, S., Fettweis, X., Gallee, H., Jouzel, J., Kageyama, M., Lerche, H., Minster, B., Picard, G., Punge, H. J., Risi, C., Salas, D., Schwander, J., Steffen, K., Sveinbjörnsdóttir, A. E., Svensson, A., and White, J.: Understanding the climatic signal in the water stable isotope records from the NEEM shallow firn/ice cores in northwest Greenland, *J. Geophys. Res.-Atmos.*, 116, D06108, doi:10.1029/2010JD014311, 2011.
- Steen-Larsen, H. C., Johnsen, S. J., Masson-Delmotte, V., Stenni, B., Risi, C., Sodemann, H., Balslev-Clausen, D., Blunier, T., Dahl-Jensen, D., Ellehj, M. D., Falourd, S., Gkinis, V., Grinsted, A., Jouzel, J., Popp, T., Sheldon, S., Simonsen, S. B., Sjolte, J., Steffensen, J. P., Sperlich, P., Sveinbjörnsdóttir, A. E., Vinther, B. M., and White, J.: Continuous monitoring of summer surface water vapour isotopic composition above the Greenland Ice Sheet, *Atmos. Chem. Phys.*, 13, 4815–4828, available at: [www.atmos-chem-phys.net/13/4815/2013/](http://www.atmos-chem-phys.net/13/4815/2013/), doi:10.5194/acp-13-4815-2013, 2013.
- Steinwagner, J., Milz, M., Von Clarmann, T., Glatthor, N., Grabowski, U., Hpfner, M., Stiller, G. P., and Reckmann, T.: HDO measurements with MIPAS, *Atmos. Chem. Phys. Discuss.*, 7, 2601–2615, available at: <http://www.atmos-chem-phys-discuss.net/7/931/2007/>, 2007.
- Tremoy, G., Vimeux, F., Mayaki, S., Souley, I., Cattani, O., Risi, C., Favreau, G., and Oi, M.: A 1-year long δ<sup>18</sup>O record of water vapor in Niamey (Niger) reveals insightful atmospheric processes at different timescales, *Geophys. Res. Lett.*, 39, L08805, doi:10.1029/2012GL051298, 2012.
- Werner, M., Heimann, M., and Hoffmann, G.: Isotopic composition and origin of polar precipitation in present and glacial climate simulations, *Tellus B*, 53, 53–71, 2001.
- Werner, M., Langebroek, P. M., Carlsen, T., Herold, M., and Lohmann, G.: Stable water isotopes in the ECHAM5 general circulation model: toward high-resolution isotope modeling on a global scale, *J. Geophys. Res.*, 16, D15109, doi:10.1029/2011JD015681, 2011.
- Worden, J., Bowman, K., Noone, D., Beer, R., Clough, S., Eldering, A., Fisher, B., Goldman, A., Gunson, M., Herman, R., Kulawik, S. S., Lampel, M., Luo, M., Osterman, G., Rinsland, C., Rodgers, C., Sander, S., Shephard, M., and Worden, H.: Tropospheric emission spectrometer observations of the tropospheric HDO/H<sub>2</sub>O ratio: estimation approach and characterization, *J. Geophys. Res.-Atmos.*, 111, D16309, doi:10.1029/2005jd006606, 2006.
- Worden, H., Beer, R., Bowman, K.W., Fisher, B., Luo, M., Rider, D., Sarkissian, E., Tremblay, D., and Zong, J.: TES Level 1 Algorithms: Interferogram Processing, Geolocation, Radiometric, and Spectral Calibration, *IEEE T. Geosci. Remote.*, 44, No.5, 1288–1296, 2006.
- Wunch, D., Toon, G. C., Wennberg, P. O., Wofsy, S. C., Stephens, B. B., Fischer, M. L., Uchino, O., Abshire, J. B., Bernath, P., Biraud, S. C., Blavier, J.-F. L., Boone, C., Bowman, K. P., Browell, E. V., Campos, T., Connor, B. J., Daube, B. C., Deutscher, N. M., Diao, M., Elkins, J. W., Gerbig, C., Gottlieb, E., Griffith, D. W. T., Hurst, D. F., Jiménez, R., Keppel-Aleks, G., Kort, E. A., Macatangay, R., Machida, T., Matsueda, H., Moore, F., Morino, I., Park, S., Robinson, J., Roehl, C. M., Sawa, Y., Sherlock, V., Sweeney, C., Tanaka, T., and Zondlo, M. A.: Calibration of the Total Carbon Column Observing Network using aircraft profile data, *Atmos. Meas. Tech.*, 3, 1351–1362, doi:10.5194/amt-3-1351-2010, 2010.

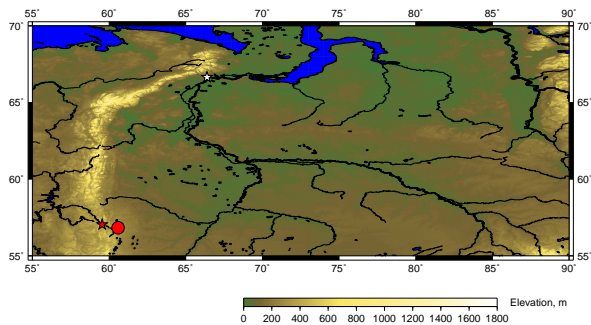


**Fig. 1.** Map of the target region (Western Siberia). Kurovka observation site is marked with red star and Yekaterinburg is marked with red circle. White star stands for future site in Labytnangi.

Wunch, D., Toon, G. C., Blavier, J.-F. L., Washenfelder, R. A., Notholt, Connor, B. J., Griffith, D. W. T., Sherlock, V., and Wennberg, P. O.: the total carbon column observing network, *Philos. T. R. Soc. A*, 369, 2087–2112, doi:10.1098/rsta.2010.0240, 2011.

Zakharov, V. I., Imasu, R., Gribanov, K. G., Hoffmann, G., and Jouzel, J.: Latitudinal distribution of the deuterium to hydrogen ratio in the atmospheric water vapor retrieved from IMG/ADEOS data, *Geophys. Res. Lett.*, 31, L12104, doi:10.1029/2004GL019433, 2004.

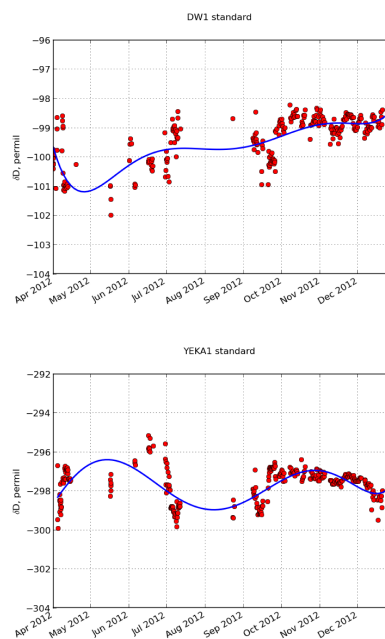


**Fig. 2.** Variability of DWI (top panel) and YEKA1 (bottom panel) standards measurements along with the polynomial fit used for calibration.

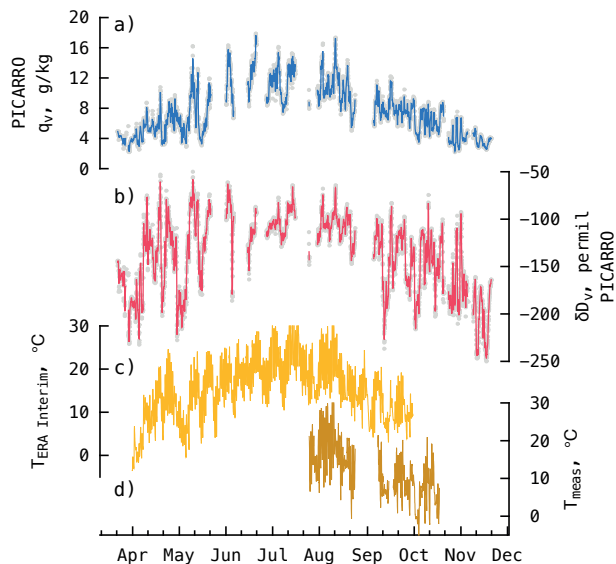


**Fig. 3.** Time series including (a) hourly (gray dots) and running (5 points, blue curve) means of specific humidity measured by PICARRO at Kourovka station, (b) hourly (gray dots) and running (5 point, red curve) means of  $\delta D$  measured by PICARRO at Kourovka, (c) local temperature derived from ERA-interim reanalysis data, (d) local temperatures measured at Kourovka by MetPak-II meteorological station.

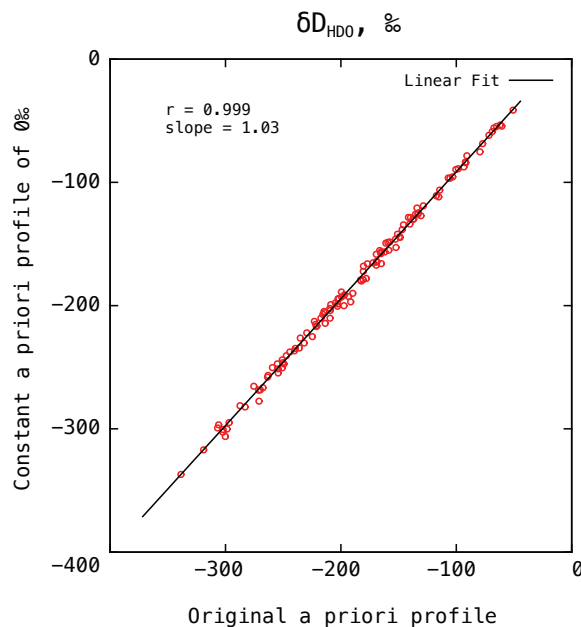


**Fig. 5.** Sensitivity of the retrieval from FTIR observations to different a-priori assumptions. Retrievals started from initial guess defined by the formula 1 are plotted vs retrievals started from constant and equal to zero initial guess  $\delta D_v$  vertical profile. Standard deviation of retrieval difference is about 1%.

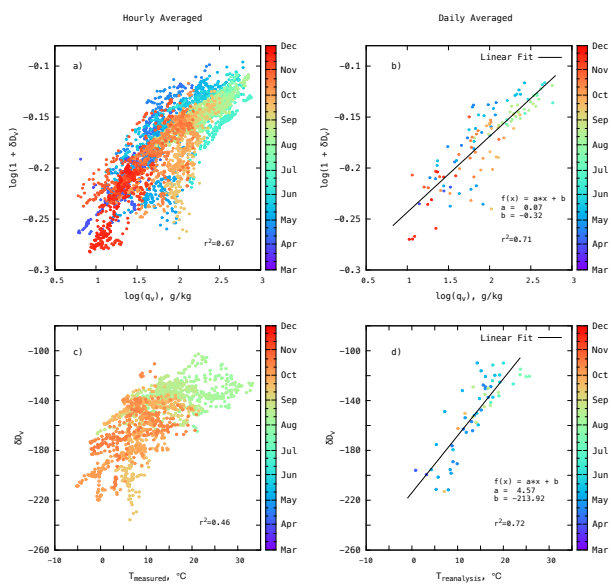


**Fig. 4.** Scatter plots for  $\ln(1 + \delta D_v)$  vs  $\ln(q_v)$ , hourly (a) and daily (b) means;  $\delta D_v$  (PICARRO) vs local temperature measured at Kourovka (c);  $\delta D_v$  (PICARRO) vs ERA-interim reanalysis temperatures (d).

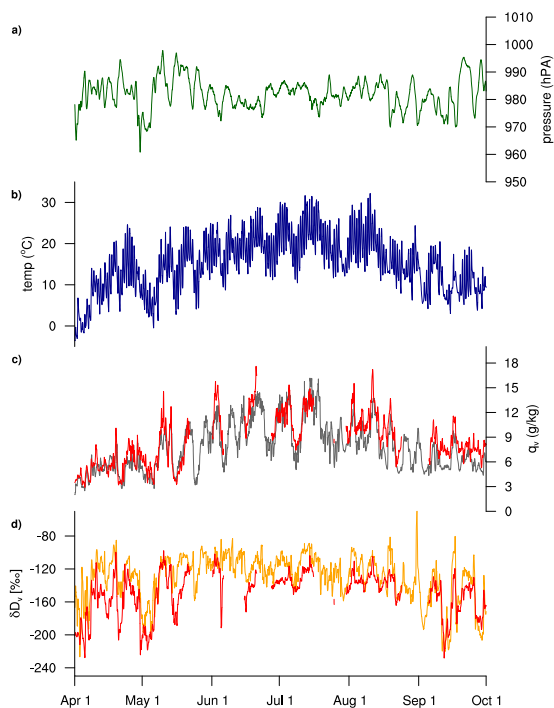


**Fig. 6.** Time series of ECHAM5-wiso simulation values between 1 April and 30 September 2012 of (a) surface pressure (green line), (b) surface temperature (blue), (c) vapour amount  $q_v$  of the lowest model grid box (grey), (d)  $\delta D$  of the water vapour (yellow). In panel (c) and d) the related smoothed PICARRO measurements (red lines) are shown for comparison, too. The model values are all taken from the grid box enclosing Kourvka station.

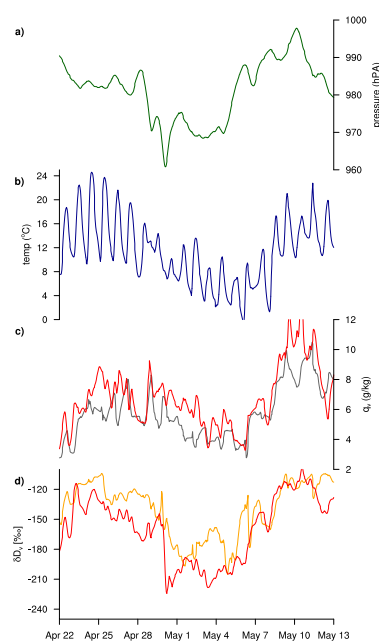


**Fig. 7.** The same as Fig. 6, but for the period 22 April to 13 May.

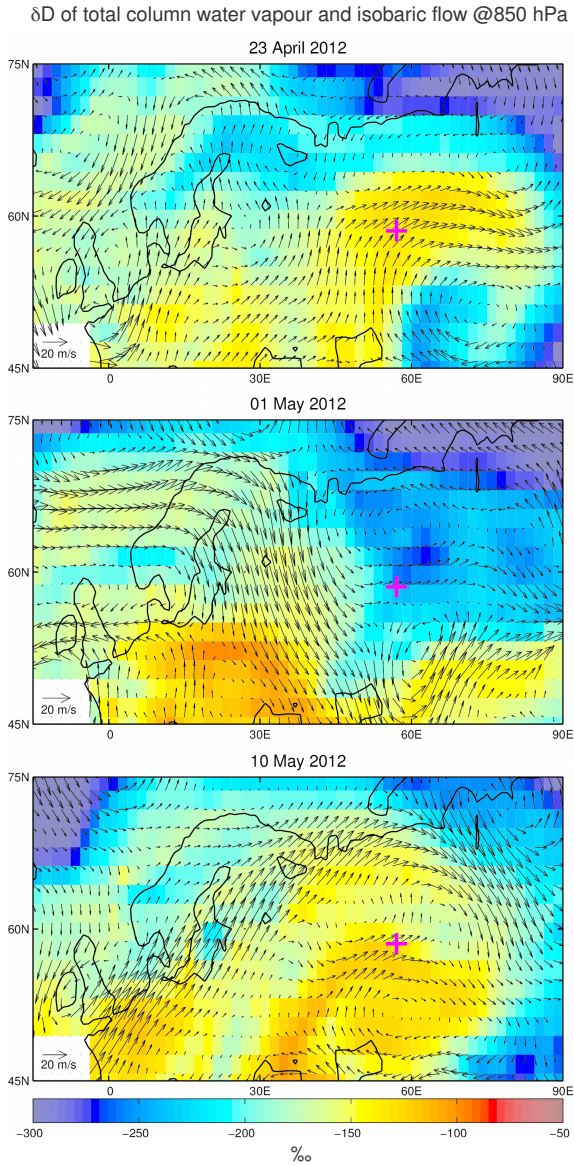


**Fig. 8.** Horizontal wind flow at 850 hPa (vectors) and  $\delta D$  composition of the total water column (colored pattern) for (a) 23 April, (b) 1 May, (c) 10 May for the region  $45^{\circ} N$ – $75^{\circ} N$ ,  $15^{\circ} W$ – $90^{\circ} E$  as simulated by ECHAM5-wiso. The location of Kourouka station is marked by red cross.

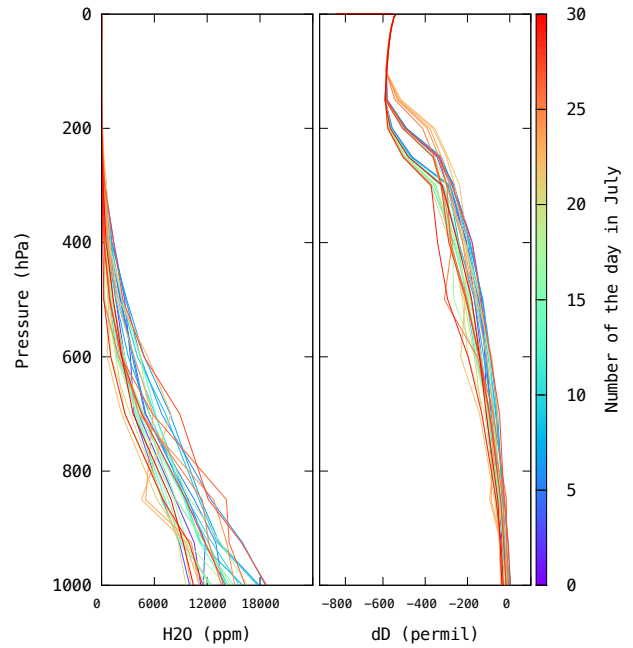


**Fig. 9.**  $H_2O$  and corresponding  $\delta D$  a-priori profiles derived from NCEP/NCAR reanalysis data using Eq. (1).

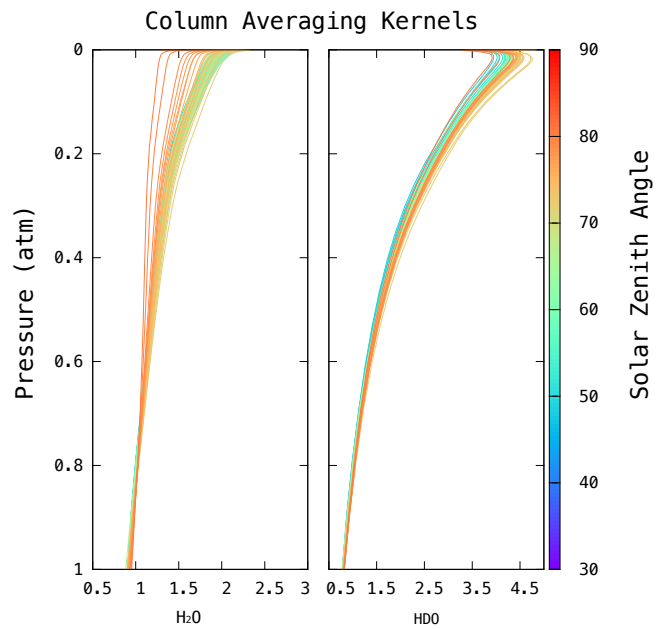


**Fig. 10.**  $H_2O$  and HDO column averaging kernels for different solar zenith angles.

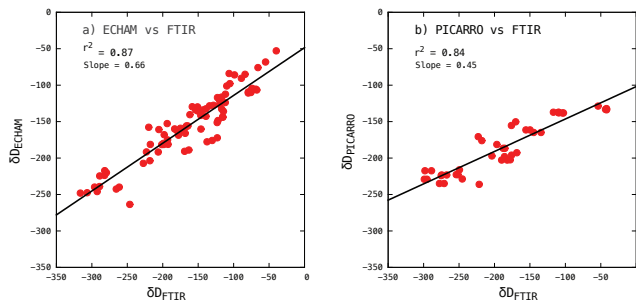


**Fig. 11.** FTIR results comparison: a) with columnar ECHAM-5-wiso  $\delta D_v$  values and b) with  $\delta D_v$  values measured by Picarro instrument at surface.